



**POLITECNICO**  
MILANO 1863



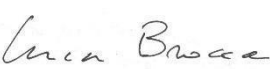
## Anthropogenic Water Use (CCI-AWU)

### **Deliverable 7:** **Product User Guide (PUG)**

Date	Issue	Section	Page	Comment
18/04/2025	1.0			

## Control Document

Process	Name	Date
Written by:	Pierre Laluet, Jacopo Dari, Sara Modanesi, Michel Bechtold, Louise Busschaert Luca Brocca, Christian Massari, Carla Saltalippi, Renato Morbideli, Gabrielle De Lannoy, Zdenko Heyvaert, Wouter Dorigo, Pia Langhans, Maria Cristina Rulli, Davide Danilo Chiarelli, Nikolas Galli	
Checked by	Luca Brocca	18/04/2025

	Signature	Date
For CCI AWU team		18/04/2025
For ESA		

[This page is left intentionally blank]

---

## List of content

1. Introduction.....	5
1.1. The CCI-AWU Project.....	5
1.2. Scope of this Report .....	5
1.3. Applicable Documents.....	6
2. Datasets Overview.....	7
3. Structure and Format of the Products.....	9
3.1. Data File Format and Naming Convention .....	9
3.2. Variables .....	9
3.3. Coordinates .....	9
4. Datasets Characteristics .....	10
4.1. Common Characteristics.....	10
4.2. Characteristics of the CONUS Datasets .....	11
4.3. Characteristics of the Ebro Basin Datasets.....	12
4.4. Characteristics of the Murray-Darling Basin Datasets.....	14
4.5. Characteristics of the India Datasets.....	15
5. Datasets Interpretation .....	16
6. Datasets Uncertainties .....	17
7. Datasets Validation.....	18
8. Key Knowledge Elements .....	18
8.1. Study Regions .....	19
8.2. Algorithms .....	20
8.2.1. SM-based Inversion .....	20
8.2.2. SM-based Delta .....	21
8.2.3. Model-observation integration (Noah-MP).....	22
8.3. Inputs data.....	22
8.3.1. Soil moisture data.....	22
Advanced Scatterometer (ASCAT).....	23
8.3.2. Evapotranspiration data .....	23
8.3.3. Maps of irrigated areas.....	24
9. Datasets Access .....	26
10. Contact Information .....	27
10. User Feedback .....	28
References .....	29

---

# 1. Introduction

## 1.1. The CCI-AWU Project

The closure of the Earth's water cycle (as well as the energy balance and the carbon cycles) through satellite Earth Observation (EO) represents one of the outstanding scientific challenges highlighted by the Global Climate Observing System (GCOS). Required standards of accuracy are fixed to 5% and annual timescale. To this end, a suite of essential climate variables (ECVs) has been defined to understand the evolution of climate and to assess the potential derived risks. However, if targets at annual timescale can generally be reached, larger uncertainties are observed for sub-annual and sub-continental time and spatial scales, respectively (Dorigo et al., 2021; Rodell et al., 2015). In this context, the development of an ECV that includes information on anthropogenic water use (AWU) can help in advancing the proper closure of the water cycle at higher spatial and temporal scales. In the ESA Climate Change Initiative Anthropogenic Water Use (CCI-AWU) precursor project, AWU is more specifically intended as agricultural water allocated for irrigation, which represents the largest anthropogenic water use, thus making irrigation the most impactful human activity on the hydrological cycle. FAO (2016) estimated that irrigation, worldwide, accounts for more than 70% of water withdrawn from the surface (i.e., rivers, lakes) and subsurface (i.e., groundwater) water sources and these estimates are expected to increase in the near future due to an increase in population and in food production, especially over arid and semi-arid regions (McDermid et al., 2023). In this context, the main data source identified by GCOS for tracking AWU is FAO's AQUASTAT. However, AQUASTAT provides survey-based irrigation estimates that do not meet the GCOS requirements, i.e., data are provided on a 5-year interval instead of yearly and are available every 2-3 years.

The overarching objective of the Climate Change Initiative – Anthropogenic Water Use (CCI-AWU) precursor project is to derive long-term (i.e., at least twenty years) AWU time series for selected regions using several approaches exploiting remote sensing observations, as a proof-of-concept of the feasibility towards a proper AWU ECV product.

The CCI-AWU project is led by a consortium coordinated by CNR-IRPI and includes the following institutions:

1. Vienna University of Technology (TU Wien) (TUWIEN)
2. KU Leuven, Department of Earth and Environmental Sciences, Division of Soil and Water Management (KULeuven)
3. University of Perugia (UNIPG)
4. Politecnico di Milano, Department of Civil and Environmental Engineering (POLIMI)

## 1.2. Scope of this Report

This Product User Guide (PUG) describes the specifications of the long-term AWU datasets produced within the framework of the CCI-AWU project, covering four key study areas: the CONUS (Continental United States), India, the Ebro Basin (in Spain), and the Murray-Darling Basin (in Australia). It provides a detailed overview of the dataset characteristics, discusses their interpretation and uncertainties, and summarizes the

validation results against in situ data and intercomparison. Key information regarding the study areas, the algorithms used for dataset generation—namely the SM-based (Soil Moisture-based) Inversion, SM-based Delta, and Model-observation integration based on Noah-MP approaches—as well as the main input datasets, is also included.

These datasets are experimental and should be used accordingly. This document is intended for scientists and modelers interested in large-scale, long-term irrigation estimates, particularly those integrating such data into hydrological, land surface, and climate models. For a comprehensive description of the satellite and reference data, processing framework, and methodologies, please refer to the Algorithm Theoretical Basis Document (ATBD). Validation results based on in situ data, along with dataset intercomparisons, can be found in the D4 Product Validation and Algorithm Assessment Report (PVSAR) and the D6 Product Validation and Intercomparison Report (PVIR).

### 1.3. Applicable Documents

- Proposal.
- Deliverable D2. Report explaining the criteria for selecting the test regions.
- Deliverable D3. Algorithm Theoretical Baseline Document (ATBD).
- Deliverable D4. Product Validation and Algorithm Selection Report (PVSAR).
- Deliverable D6. Product Validation and Intercomparison Report (PVIR).

All deliverables mentioned here will be made publicly available at the following link:  
<https://climate.esa.int/en/projects/anthropogenic-water-use/>.

## 2. Datasets Overview

Table 1 provides an overview of the datasets produced within the CCI-AWU project at a 0.25° spatial resolution, detailing their temporal coverage and availability across the four study regions.

Three distinct approaches were employed: SM-based Delta (Zaussinger et al., 2019; Zappa et al., 2021, 2022, 2024), SM-based Inversion (Brocca et al., 2018; Jalilvand et al., 2019; Dari et al., 2020, 2022, 2023), and the Model-observation integration approach based on the Noah-MP v4.0.1 land surface model (Niu et al., 2011), coupled with a sprinkler irrigation scheme (Ozdogan et al., 2010) and overlaid with irrigated area maps derived from satellite observations.

The "Dataset" column in Table 1 lists the various AWU datasets generated by each method, based on different SM and evapotranspiration (ET) input datasets. The red cells indicate regions where Model-Observation Integration datasets are unavailable. The SM-based Inversion method uses five different SM datasets: CCI Combined, CCI Passive, Advanced Scatterometer (ASCAT), Soil Moisture and Ocean Salinity (SMOS), and Soil Moisture Active Passive (SMAP). The SM-based Delta method relies on three SM datasets (CCI Combined, CCI Passive, CCI Active) and two ET datasets (FLUXCOM, SSEBOP). The Model-observation integration (Noah-MP) method includes three different datasets using different irrigated area maps: one derived from Landsat observations (Teluguntla et al., 2023), referred to as "Landsat"; one based on the "Relative Bias" approach described in ATBD Section 5.2.1, referred to as "Method 1"; and another based on the "Multi-Resolution Analysis Approach" described in ATBD Section 5.2.2, referred to as "Method 2".

**Table 1:** The AWU datasets with their time coverage and availability for each region

Method	Dataset	Data availability	CONUS	Ebro basin	Murray-Darling basin	India
SM-based Delta	CCI Combined & FLUXCOM	2003-2020				
	CCI Passive & FLUXCOM	2003-2020				
	CCI Active & FLUXCOM	2003-2020				
	CCI Combined & SSEBOP	2003-2022				
	CCI Passive & SSEBOP	2003-2022				
	CCI Active & SSEBOP	2003-2022				
SM-based	CCI Combined	2003-2022				

Inversion	CCI Passive	2003-2022				
	ASCAT	2003-2022				
	SMOS	2010-2022				
	SMAP	2015-2022				
Model- observation integration (Noah-MP)	Landsat	2010-2022				
	Method 1	2010-2022				
	Method 2	2010-2022				



## 3. Structure and Format of the Products

### 3.1. Data File Format and Naming Convention

The data is stored in NetCDF format, following a standardized naming convention:

**AWU\_<method>\_<site>\_<product>.nc**

- **<method>** refers to the dataset generation approach, which includes "SM\_Delta" for the SM-based Delta method, "SM\_Inversion" for the SM-based Inversion method, and "NoahMP" for the Model-observation integration approach.
- **<site>** identifies the four study regions: "CONUS" for the Contiguous United States, "Murray" for the Murray-Darling Basin, "Ebro" for the Ebro Basin, and "India".
- **<product>** varies depending on the dataset type (SM data, ET data, and irrigated area maps) used. For the SM-based Delta method, products include "CCI\_Combined\_FLUXCOM", "CCI\_Passive\_FLUXCOM", "CCI\_Active\_FLUXCOM", "CCI\_Combined\_SSEBOP", "CCI\_Passive\_SSEBOP", and "CCI\_Active\_SSEBOP". For the SM-based Inversion method, products include "CCI\_Combined", "CCI\_Passive", "ASCAT", "SMOS", and "SMAP". For the Model-observation integration method, the products are "Landsat", "Method1", and "Method2".

### 3.2. Variables

- For the SM-based Inversion and SM-based Delta datasets:
  - **Irrigation** [mm/month]
- For the Model-observation integration (Noah-MP) datasets:
  - **IWU\_ensmean** [mm/month]
  - **IWU\_uncertainty** [mm/month]

### 3.3. Coordinates

- **time**: Represents the date of the irrigation data stored in the NetCDF file. The format is YYYY-MM-DD, where YYYY is the four-digit year, MM is the two-digit month (ranging from 01 to 12), and DD corresponds to the last day of the respective month.
- **lon** [degree]: Longitude coordinate.
- **lat** [degree]: Latitude coordinate.

## 4. Datasets Characteristics

### 4.1. Common Characteristics

**Table 2:** Characteristics common to all irrigation datasets.

<b>Coordinate System</b>	Geographic
<b>Datum</b>	WGS84
<b>File Format</b>	NetCDF
<b>Pixel Size</b>	0.25°
<b>Temporal Frequency</b>	Monthly
<b>Units</b>	mm/month
<b>Fill Value</b>	NaN
<b>Scale Factor</b>	N/A
<b>Valid Range</b>	All values are valid

## 4.2. Characteristics of the CONUS Datasets

**Table 3:** Characteristics of irrigation datasets of the CONUS region.

File name	Temporal extent	Spatial extent	Columns /Rows	File size	Layer 1	Layer 2	Temporal mask	Data type
AWU_SM_Delta_CONUS_CCI_Active_FLUXCOM	2003-2020	Lat: 25.38°N – 49.12°N Lon: -124.6°W – -67.12°W	231 (lon) / 96 (lat)	38.8 MB	Irrigation	N/A	October-April	float64
AWU_SM_Delta_CONUS_CCI_Combined_FLUXCOM	2003-2020			38.3 MB				
AWU_SM_Delta_CONUS_CCI_Passive_FLUXCOM	2003-2020			38.8 MB				
AWU_SM_Delta_CONUS_CCI_Active_SSEBOP	2003-2022			41.4 MB				
AWU_SM_Delta_CONUS_CCI_Combined_SSEBOP	2003-2022			41.4 MB				
AWU_SM_Delta_CONUS_CCI_Passive_SSEBOP	2003-2022			41.4 MB				
AWU_SM_Inversion_CONUS_ASCAT	2007-2022	Lat: 24.88°N – 49.38°N Lon: -124.9°W – -66.88°W	233 (lon) / 99 (lat)	17.7 MB	Irrigation	N/A	October-April	float32
AWU_SM_Inversion_CONUS_CCI_Combined	2003-2022			22.2 MB				
AWU_SM_Inversion_CONUS_CCI_Passive	2003-2022			22.2 MB				
AWU_SM_Inversion_CONUS_SMAP	2015-2022			8.6 MB				
AWU_SM_Inversion_CONUS_SMOS	2010-2022			13.9 MB				

AWU_NoahMP_CONUS_Landsat	2010-2022	Lat: 24.88°N – 49.38°N Lon: -124.9°W – -66.88°W	233 (lon) / 99 (lat)	10.2 MB	IWU_ensmean	IWU_uncertainty	Based on the greenness vegetation fraction from AVHRR	float64
AWU_NoahMP_CONUS_Method1	2010-2022			3.2 MB				
AWU_NoahMP_CONUS_Method2	2010-2022			0.7 MB				

## 4.3. Characteristics of the Ebro Basin Datasets

**Table 4:** Characteristics of irrigation datasets of the Ebro Basin region.

File name	Temporal extent	Spatial extent	Columns/Rows	File size	Layer	Temporal mask	Data type
AWU_SM_Delta_Ebro_CCI_Active_FLUXCOM	2003-2020	Lat: 40.62°N – 43.12°N Lon: -3.875°W – 1.875°W	24 (lon) / 11 (lat)	0.46 MB	Irrigation	November-March	float64
AWU_SM_Delta_Ebro_CCI_Combined_FLUXCOM	2003-2020			0.46 MB			
AWU_SM_Delta_Ebro_CCI_Passive_FLUXCOM	2003-2020			0.46 MB			
AWU_SM_Delta_Ebro_CCI_Active_SSEBOP	2003-2022			0.46 MB			
AWU_SM_Delta_Ebro_CCI_Combined_SSEBOP	2003-2022			0.46 MB			
AWU_SM_Delta_Ebro_CCI_Passive_SSEBOP	2003-2022			0.46 MB			
AWU_SM_Inversion_Ebro_ASCAT	2007-2022	Lat:	29 (lon) / 14 (lat)	0.32 MB	Irrigation	November-March	float32



## Anthropogenic Water Use (CCI-AWU)

4000142449/23/I-NB

Page 13

---

AWU_SM_Inversion_Ebro_CCI_Combined	2003-2022	40.12°N – 43.38°N Lon: -4.625°W – 2.375°W		0.40 MB			
AWU_SM_Inversion_Ebro_CCI_Passive	2003-2022			0.40 MB			
AWU_SM_Inversion_Ebro_SMAP	2015-2022			0.16 MB			
AWU_SM_Inversion_Ebro_SMOS	2010-2022			0.26 MB			

## 4.4. Characteristics of the Murray-Darling Basin Datasets

**Table 5:** Characteristics of irrigation datasets of the Murray-Darling Basin region.

File name	Temporal extent	Spatial extent	Columns/ Rows	File size	Layer 1	Layer 2	Temporal mask	Data type
AWU_SM_Delta_Murray_CCI_Active_FLUXCOM	2003-2020	Lat: -37.62°N – -24.62°N Lon: 138.6°W – 152.4°W	56 (lon) / 53 (lat)	5.1 MB	Irrigation	N/A	May-August	float64
AWU_SM_Delta_Murray_CCI_Combined_FLUXCOM	2003-2020			5.1 MB				
AWU_SM_Delta_Murray_CCI_Passive_FLUXCOM	2003-2020			5.1 MB				
AWU_SM_Delta_Murray_CCI_Active_SSEBOP	2003-2022			5.5 MB				
AWU_SM_Delta_Murray_CCI_Combined_SSEBOP	2003-2022			5.5 MB				
AWU_SM_Delta_Murray_CCI_Passive_SSEBOP	2003-2022			5.5 MB				
AWU_SM_Inversion_Murray_ASCAT	2007-2022	Lat: -37.88°N – -24.38°N Lon: 138.4°W – 152.6°W	58 (lon) / 55 (lat)	2.5 MB	Irrigation	N/A	April-August	float32
AWU_SM_Inversion_Murray_CCI_Combined	2003-2022			3.1 MB				
AWU_SM_Inversion_Murray_CCI_Passive	2003-2022			3.1 MB				
AWU_SM_Inversion_Murray_SMAP	2015-2022			1.2 MB				
AWU_SM_Inversion_Murray_SMOS	2010-2022			1.9 MB				

AWU_NoahMP_Murray_Landsat	2010-2022	Lat: -37.88°N – - 24.38°N Lon: 138.4°W – 152.6°W	58 (lon) / 55 (lat)	1.7 MB	IWU_ensmean	IWU_uncertainty	May-August	float64
---------------------------	-----------	--	------------------------	--------	-------------	-----------------	------------	---------

## 4.5. Characteristics of the India Datasets

**Table 6:** Characteristics of irrigation datasets of the India region.

File name	Temporal extent	Spatial extent	Columns/Rows	File size	Layer	Temporal mask	Data type
AWU_SM_Delta_Ebro_CCI_Active_FLUXCOM	2003-2020	Lat: 8.125°N – 34.88°N Lon: 68.38°W – 94.88°W	108 (lon) / 107 (lat)	19.6 MB	Irrigation	July-October (monsoon season)	float64
AWU_SM_Delta_Ebro_CCI_Combined_FLUXCOM	2003-2020			19.6 MB			
AWU_SM_Delta_Ebro_CCI_Passive_FLUXCOM	2003-2020			19.6 MB			
AWU_SM_Inversion_Ebro_ASCAT	2007-2022	Lat: 7.875°N – 37.12°N Lon: 68.12°W – 97.62°W	118 (lon) / 119 (lat)	10.8 MB	Irrigation	July-October (monsoon season)	float32
AWU_SM_Inversion_Ebro_CCI_Combined	2003-2022			13.5 MB			
AWU_SM_Inversion_Ebro_CCI_Passive	2003-2022			13.5 MB			
AWU_SM_Inversion_Ebro_SMAP	2015-2022			5.2 MB			
AWU_SM_Inversion_Ebro_SMOS	2010-2022			8.5 MB			

## 5. Datasets Interpretation

The datasets provide estimates of the water applied for irrigation. They are experimental and should be interpreted accordingly. While they have been validated against in situ data in the CONUS, the Murray-Darling basin, and the Ebro basin (see D4 PVASR sections 2.1 and 3.4 for the Murray-Darling basin, sections 2.2, 3.2, and 5.3 for CONUS, and sections 2.4 and 3.3 for the Ebro basin) and intercompared (see D6 PVIR), they offer valuable insights into long-term and large-scale irrigation practices and represent a significant step toward the quantification of irrigation at these scales. However, our knowledge of their performance in comparison to actual irrigation practices remains limited to the regions and periods for which in situ data are available, as well as to comparisons with auxiliary datasets (irrigated area extent, climate) and intercomparison of dataset dynamics.



## 6. Datasets Uncertainties

The datasets derived from the Model-observation integration (Noah-MP) approach include an uncertainty estimate based on an ensemble of 24 simulations, obtained by perturbing the meteorological input data. The uncertainties are provided in the variable "IWU\_uncertainty" within the Model-observation integration (Noah-MP) datasets. Further details on the uncertainty estimation methodology can be found in ATBD Section 5.3.3. The datasets produced using the SM-based Inversion and SM-based Delta approaches do not include an uncertainty estimate.

---

## 7. Datasets Validation

The datasets were validated using in situ data, including annual state-level irrigation records for the CONUS (2013 and 2018) and monthly district-level irrigation data for the Ebro and Murray-Darling Basins. Detailed analyses are provided in D4 PVASR, while dataset intercomparison and evaluation with auxiliary data are presented in D6 PVIR.

**In the CONUS**, the NOAH-MP datasets demonstrate the best agreement with in situ data, followed by SM-INVERSION (CCI Passive). The SM-DELTA (CCI Passive & FLUXCOM) dataset also performs well but tends to overestimate irrigation. Regarding spatial pattern, NOAH-MP (Landsat) and SM-DELTA (CCI Passive) show the highest alignment with a map of the percentage of area equipped for irrigation in the four most irrigated regions (California Valley, Snake River Plain, Mississippi Floodplain, and the Great Plains). These two datasets also capture similar temporal dynamics, including wet and dry years, despite relying on independent methodologies and input datasets.

**In the Ebro Basin**, all datasets show an underestimation of irrigation when compared to in situ data. Metrics are relatively similar across the SM-DELTA datasets. SM-INVERSION datasets generally display stronger underestimation and lower Pearson correlations compared to SM-DELTA, with the exception of CCI Passive, which performs comparably. Regarding spatial patterns, SM-DELTA datasets exhibit some correlation with the percentage of area equipped for irrigation, whereas SM-INVERSION does not. Nevertheless, in terms of temporal dynamics, SM-DELTA (CCI Combined & FLUXCOM, CCI Passive & FLUXCOM) and SM-INVERSION (CCI Combined, CCI Passive) show strong similarities, despite differences in algorithms and input datasets.

**In the Murray-Darling Basin**, performance varies widely between districts, with no dataset consistently standing out. SM-DELTA datasets using SSEBOP ET and SM-INVERSION (CCI Passive) tend to perform better in Murrumbidgee and Coleambally, while NOAH-MP (Landsat) shows better results in Murray Mulwala and Coleambally. Regarding spatial patterns, NOAH-MP (Landsat) exhibits the strongest correlation with the percentage of area equipped for irrigation, while SM-DELTA datasets using FLUXCOM ET show only weak correlations. Other datasets do not exhibit any clear spatial relationship. In terms of temporal dynamics, SM-DELTA (CCI Passive and CCI Combined) closely aligns with SM-INVERSION (CCI Passive and CCI Combined).

**In India**, SM-based Inversion datasets estimate higher irrigation levels, especially during the Rabi season (November-March), than the SM-based Delta datasets. All datasets estimate more irrigation in the highly irrigated Ganges Valley in the north. Spatially, SM-based Delta datasets show a correlation with a map of irrigated areas, while the SM-based Inversion ones do not.

---

## 8. Key Knowledge Elements

To provide users with essential knowledge, we summarize below the key information regarding the study regions, the algorithms employed, and the satellite data and models utilized. For further details on the study areas, please refer to the D2 Report explaining the criteria for selecting test region, D3 ATBD, and D4 PVASR.

### 8.1. Study Regions

Figure 1 illustrates the four study regions for which irrigation datasets have been generated. The  $0.25^\circ$  pixels displayed on the maps represent the percentage of irrigation equipment within each pixel, derived from the Global Map of Irrigated Area by Siebert et al. (2013). There are significant differences in the density of irrigated areas and the spatial distribution of irrigation across these regions.

In the CONUS, irrigation is primarily concentrated in four highly irrigated zones. From west (more arid) to east (more humid): the California Valley, Snake River Plain, Great Plains, and Mississippi Floodplains. In the Ebro Basin, irrigation is mainly concentrated in the eastern part of the Ebro Valley, where sprinkler, drip, and flood irrigation are intensively practiced. In the Murray-Darling Basin, which has a semi-arid climate, irrigation is predominantly located in the south along the Murray River, with additional irrigated areas in the northeast. In India, the Ganges Valley in the north is the most intensely irrigated region globally. The rest of India also has extensive irrigation coverage. There are three irrigation seasons in India: Rabi (dry season, November to March), Zaid (intermediate season, April to May), and Kharif (monsoon season, June to October).

## Areas Equipped for Irrigation (GMIA) by Region

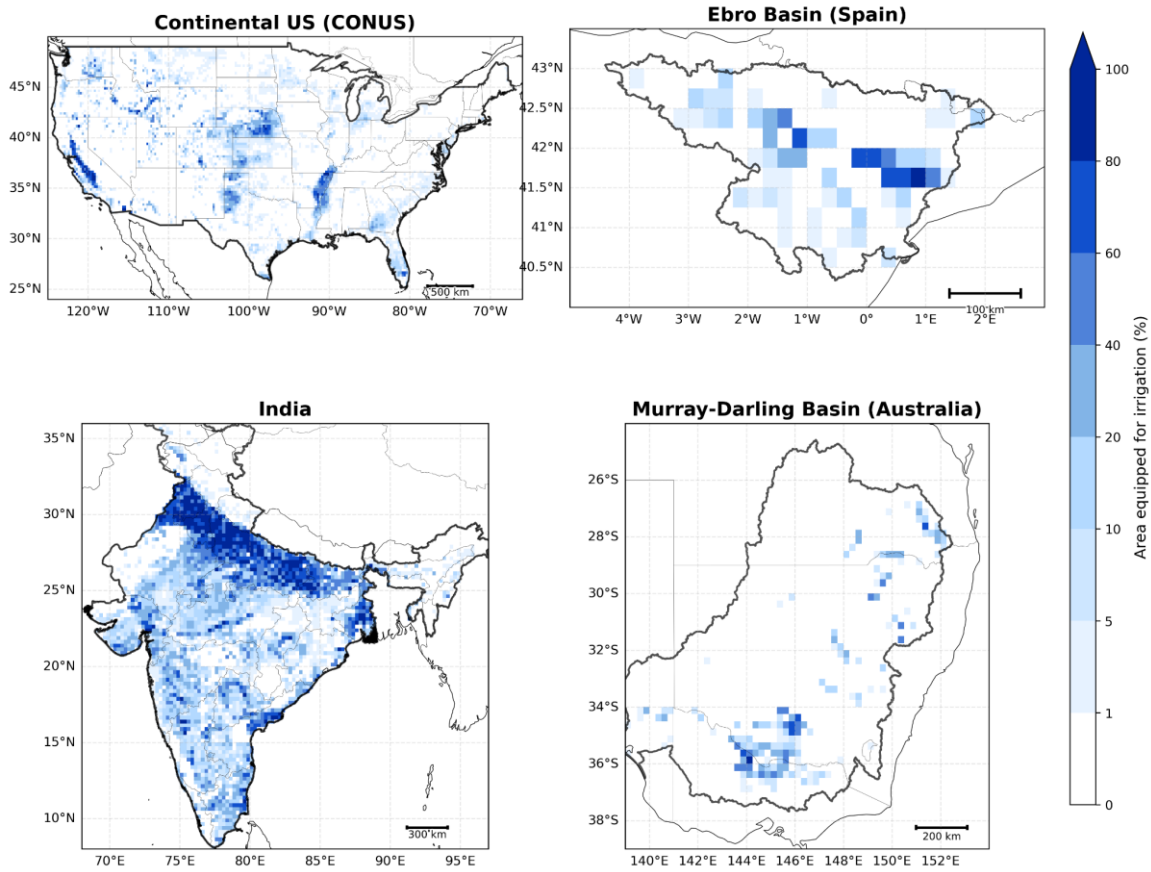


**Figure 1:** Four study regions for which irrigation datasets were produced (CONUS, Ebro Basin, India, and Murray-Darling Basin) with the percentage of area equipped for irrigation (GMIA; Siebert et al., 2013).

## 8.2. Algorithms

### 8.2.1. SM-based Inversion

The SM-based Inversion approach estimates irrigation water use by inverting the soil water balance equation. This method, derived from the SM2RAIN algorithm (Brocca et al., 2014), uses SM variations to distinguish between precipitation and irrigation water inputs. By removing precipitation from the estimated water input, the irrigation contribution can be isolated.

The soil water balance equation is expressed as:

$$nZ \frac{dS(t)}{dt} = i(t) + r(t) - g(t) - sr(t) - e(t) \quad (\text{Eq. 1})$$

In which  $n$  [-] is the soil porosity,  $Z$  [mm] is the soil layer depth,  $dS(t)/dt$  [-] is the variation of relative SM  $S(t)$  in time  $t$  [day],  $i(t)$  [mm/day] is the irrigation rate,  $r(t)$  [mm/day] is the rainfall rate,  $g(t)$  [mm/day] is the drainage,  $sr(t)$  [mm/day] is the surface runoff, and  $e(t)$  [mm/day] is the actual evapotranspiration rate.

$i(t)$  is unknown and estimated from the equation reformulated as:

$$Win(t) = Z * dS(t)/dt + g(t) + sr(t) + e(t) \quad (\text{Eq. 2})$$

with  $Win(t) = i(t) + r(t)$ , meaning irrigation is retrieved as:

$$i(t) = Win(t) - r(t) \quad (\text{Eq. 3})$$

The drainage term,  $g(t)$ , represents water percolating downward beyond the root zone and is modeled using the function  $g(t) = aS(t)^b$ , where  $a$  and  $b$  are calibration parameters (Brocca et al., 2014). The ET term,  $e(t)$ , accounts for water loss due to plant transpiration and soil evaporation. It is expressed as  $e = FS(t)pe$ , where  $pe(t)$  is the potential evapotranspiration and  $F$  is a scaling factor accounting for SM availability. Surface runoff  $sr(t)$  is considered negligible. The model parameters are calibrated on non-rainy days.

## 8.2.2. SM-based Delta

The SM-based Delta approach estimates irrigation by comparing satellite-derived SM changes  $dSM_{sat}/dt$  with modeled SM changes  $dSM_{mod}/dt$  (Zaussinger et al., 2019). The key assumption is that modeled SM changes are only driven by precipitation, while satellite SM changes reflect both precipitation and irrigation. The soil water balance equations are:

$$Z \cdot \frac{dSM_{sat}}{dt} = P(t) + I(t) - ET(t) - R(t) - \Delta S_{rest} \quad (\text{Eq. 1})$$

$$Z \cdot \frac{dSM_{mod}}{dt} = P(t) - ET(t) - R(t) - \Delta S_{rest} \quad (\text{Eq. 2})$$

where  $P(t)$  [mm] is precipitation,  $I(t)$  [mm] is irrigation,  $ET(t)$  [mm] is evapotranspiration,  $R(t)$  [mm] is runoff, and  $\Delta S_{rest}$  [mm] represents soil water storage changes. Since  $P$ ,  $ET$ ,  $R$ , and  $\Delta S_{rest}$  are assumed identical in both equations, irrigation is estimated as:

$$I(t) = Z \cdot \frac{dSM_{sat}}{dt} - Z \cdot \frac{dSM_{mod}}{dt} \quad (\text{Eq. 3})$$

Zappa et al. (2022b, 2024) improved the method by incorporating  $ET$  [mm] differences between satellite (including irrigation signal) and model (excluding irrigation signal). This latest version was used in the CCI-AWU project. The refined equation accounts for this as follows:

$$I = Z * \frac{dSM_{sat}}{dt} - Z * \frac{dSM_{mod}}{dt} + (ET_{w/irrig}(t) - ET_{w/o\_irrig}(t)) \quad (\text{Eq. 4})$$

Where  $ET_{w/irrig}$  [mm] is the ET data theoretically including irrigation, and  $ET_{w/o\_irrig}$  [mm] is the one theoretically excluding it.

### 8.2.3. Model-observation integration (Noah-MP)

The Model-observation integration method estimates irrigation using Noah-MP v4.0.1 (Niu et al., 2011), a land surface model embedded within NASA's Land Information System (LIS). This approach integrates satellite-derived irrigated area maps with modeled irrigation simulations.

Irrigation is simulated using a sprinkler irrigation scheme (Ozdogan et al., 2010) applied to cropland pixels identified from MODIS land cover maps. During the growing season, irrigation is triggered when root-zone moisture availability (MA) falls below a user-defined threshold ( $Th_{irr} = 0.45$ ), based on Modanesi et al. (2022), Busschaert et al. (2023), and De Lannoy et al. (2024). More information about  $Th_{irr}$  and the choice of the value 0.45 can be found in D4 PVASR.  $MA$  is defined as:

$$MA = \frac{\theta - \theta_{WP}}{\theta_{FC} - \theta_{WP}} \quad (\text{Eq. 5})$$

where  $\theta$  is the actual SM,  $\theta_{FC}$  is the wilting point, and  $\theta_{WP}$  is the field capacity associated with the soil textures derived from the Harmonized World Soil Database (HWSD). The irrigation amount restores the root-zone moisture to field capacity.

Noah-MP simulations were conducted on all cropland pixels, regardless of actual irrigation status. To refine irrigation estimates, pixel-level simulations were overlaid with three different irrigated area maps:

1. Landsat-Derived Global Rainfed and Irrigated-Cropland Product (Teluguntla et al., 2023)
2. Relative Bias Approach (D3 ATBD 5.2.1) (referred to as "Method 1"): based on bias differences between Noah-MP SM (excluding irrigation) and SMOS SM (including irrigation).
3. Multi-Resolution Analysis Approach (D3 ATBD 5.2.2) (referred to as "Method 2"): derived from spectral differences between Noah-MP SM and SMOS SM.

The overlay process adjusts irrigation estimates per pixel based on the irrigated-to-total cropland ratio. If irrigation covers only part of a grid cell, the estimated irrigation amount is reduced accordingly. Conversely, if the irrigated fraction is larger than the modeled cropland, irrigation is scaled up.

## 8.3. Inputs data

### 8.3.1. Soil moisture data

#### ESA Climate Change Initiative (CCI)

The ESA CCI SM products (CCI Active, CCI Passive, and CCI Combined; Dorigo et al., 2017) provide global SM data at a 0.25° grid resolution.

- CCI Active merges data from three radar satellites (including ASCAT from 2007) and covers the period from 1978 to the present.
- CCI Passive integrates data from 12 radiometer satellites and is available from 1978 onward.
- CCI Combined merges both CCI Active and CCI Passive datasets, also covering the period from 1978 to the present.

---

CCI Passive, CCI Combined, and CCI Active are used in the SM-based Delta algorithm, while CCI Passive and CCI Combined are used in the SM-based Inversion algorithm.

**Soil Moisture and Ocean Salinity (SMOS)**

The Soil Moisture and Ocean Salinity (SMOS) mission (Kerr et al., 2016) by ESA, launched in 2009, provides SM observations up to 5 cm depth using passive L-band microwave sensors. SMOS provides SM data at a spatial resolution of ~42 km from 2010, with a global revisit time of 3 days. SMOS data have been resampled to the ESA CCI 0.25° grid and are used in the SM-based Inversion algorithm.

**Soil Moisture Active Passive (SMAP)**

The Soil Moisture Active Passive (SMAP) mission (Entekhabi et al., 2010) by NASA provides SM observations up to 5 cm depth using passive L-band microwave sensors. The data are available at a spatial resolution of ~40 km from 2015, with a global revisit time of 3 days. SMAP data have been resampled to the ESA CCI 0.25° grid and are used in the SM-based Inversion algorithm.

**Advanced Scatterometer (ASCAT)**

The Advanced Scatterometer (ASCAT), onboard the MetOp series of satellites operated by EUMETSAT, is an active microwave radar instrument designed to measure SM globally (Brocca et al., 2017). ASCAT provides C-band backscatter observations, which are used to estimate SM at a spatial resolution of ~25 km, with a daily global coverage. The dataset is available from 2007 and has been resampled to the ESA CCI 0.25° grid. ASCAT SM data are used in the SM-based Inversion algorithm.

**ERA5-Land**

ERA5-Land is the land component of the fifth-generation European ReAnalysis (ERA5) dataset (Muñoz-Sabater, 2019), developed by the Copernicus Climate Change Service (C3S) at ECMWF. It provides land surface water and energy cycle data from 1950 at a 9 km spatial resolution with hourly time steps. Unlike satellite-based SM observations, which capture actual surface conditions, ERA5-Land does not include irrigation signals, as it is mainly driven by meteorological forcing. In this study, the 0–7 cm soil water layer is used to ensure consistency with satellite sensor depths. ERA5-Land SM data have been resampled to the ESA CCI 0.25° grid and are utilized in the SM-based Delta algorithm.

**8.3.2. Evapotranspiration data****Operational Simplified Surface Energy Balance (SSEBop)**

The Simplified Surface Energy Balance operational (SSEBop) product (Senay et al., 2018) estimates ET using a simplified energy balance approach based on the classification of “wet” and “dry” reference pixels. Wet pixels correspond to well-watered vegetation areas with high ET, while dry pixels represent bare soil or stressed vegetation with minimal ET. SSEBop scales ET values across different landscapes using surface

temperature data and is available at a spatial resolution of 1 km. SSEBOP ET data have been resampled to the ESA CCI 0.25° grid and are used in the SM-based Delta algorithm.

### **FLUXCOM**

The FLUXCOM ET product (Jung et al., 2019) is derived from a machine-learning-based model trained on ET flux tower measurements. It uses remote sensing predictors, primarily from MODIS, including vegetation indices and surface temperature. The dataset consists of outputs from 36 different machine-learning models that estimate ET at the global scale at a 0.1° resolution, resampled to 0.25°, and is used in the SM-based Delta algorithm. FLUXCOM ET data have been resampled to the ESA CCI 0.25° grid and are used in the SM-based Delta algorithm.

### **Noah-Multiparameterization (Noah-MP)**

The Noah-Multiparameter (Noah-MP) land surface model simulates ET, and for this project, we ensured that only ERA5 forecast meteorological data were used to prevent any observational influence that could introduce an irrigation signal. Consequently, unlike ET estimates from SSEBop and FLUXCOM, Noah-MP ET used here excludes irrigation effects. Noah-MP ET data have been available since 2010 for CONUS and the Murray-Darling Basin, with a 0.25° resolution, and are used in the SM-based Delta algorithm.

### **ERA5-Land**

The ERA5-Land ET dataset is used for regions and periods where Noah-MP ET data are unavailable. Analyses showed that ERA5-Land ET exhibits a very similar spatio-temporal dynamic and magnitude to Noah-MP ET, making it suitable to represent ET without irrigation. ERA5-Land ET data have a 9 km resolution, have been resampled to the ESA CCI 0.25° grid, and are used in the SM-based Delta algorithm.

### **Global Land Evaporation Amsterdam Model (GLEAM) v3.7b**

The GLEAM product (Martens et al., 2017) estimates potential evapotranspiration (PET) using a Priestley-Taylor-based formulation. It relies on satellite-derived radiation and meteorological reanalysis data to compute PET at the global scale. ETP data from GLEAM have a 0.25° resolution and are used to compute the ET term in the SM-based inversion approach.

## **8.3.3. Maps of irrigated areas**

### **Global Map of Irrigated Areas (GMIA)**

The Global Map of Irrigated Areas (GMIA) by Siebert et al. (2013) is a global dataset of the percentage of land equipped for irrigation at a 0.083° (~10 km) resolution. It was produced by compiling national and subnational irrigation statistics, integrating land cover data, proximity to water sources, and remote sensing information, and applying a downscaling method to distribute irrigation areas spatially. The dataset represents irrigation infrastructure availability, not necessarily the actual irrigated area. GMIA is used to spatially mask pixels that are non-irrigated or have low irrigation coverage (<5% equipped for irrigation) in the SM-based Inversion and SM-based Delta approaches.



### **Landsat-derived Global Rainfed and Irrigated-Cropland Product at 30 m (LGRIP30)**

The Landsat-Derived Global Rainfed and Irrigated-Cropland Product at 30 m (LGRIP30), developed by Teluguntla et al. (2023), is a high-resolution global map that distinguishes irrigated and rainfed croplands at 30-meter spatial resolution. This dataset was generated by combining the Global Cropland Extent Product at 30 m (GCEP30) ([lpdaac.usgs.gov](https://lpdaac.usgs.gov)), which identifies cropland extent, with multispectral bands and indices derived from Landsat 8 imagery for the period 2014–2017. The approach leverages supervised machine learning algorithms, such as random forests, to classify irrigated and non-irrigated areas. This map is used in the Model-observation integration algorithm.

## 9. Datasets Access

The AWU products are freely available for download at the following Zenodo link:  
<https://zenodo.org/records/14988198>

---

## 10. Contact Information

The contact email address is: [pierre.laluet@geo.tuwien.ac.at](mailto:pierre.laluet@geo.tuwien.ac.at) .

## 10. User Feedback

User feedback is warmly welcomed and encouraged. All questions and remarks concerning the product can be addressed to our contact e-mail address provided in Section 8.

---

## References

- Brocca, L., Ciabatta, L., Massari, C., Moramarco, T., Hahn, S., Hasenauer, S., Kidd, R., Dorigo, W., Wagner, W., Levizzani, V., 2014. Soil as a natural rain gauge: Estimating global rainfall from satellite soil moisture data. *Journal of Geophysical Research: Atmospheres* 119, 5128–5141. <https://doi.org/10.1002/2014JD021489>
- Brocca, L., Crow, W.T., Ciabatta, L., Massari, C., de Rosnay, P., Enenkel, M., Hahn, S., Amarnath, G., Camici, S., Tarpanelli, A., Wagner, W., 2017. A Review of the Applications of ASCAT Soil Moisture Products. *IEEE Journal of Selected Topics in Applied Earth Observations and Remote Sensing* 10, 2285–2306. <https://doi.org/10.1109/JSTARS.2017.2651140>
- Brocca, L., Tarpanelli, A., Filippucci, P., Dorigo, W., Zaussinger, F., Gruber, A., Fernández-Prieto, D., 2018. How much water is used for irrigation? A new approach exploiting coarse resolution satellite soil moisture products. *International Journal of Applied Earth Observation and Geoinformation* 73, 752–766. <https://doi.org/10.1016/j.jag.2018.08.023>
- Busschaert, L., Bechtold, M., Modanesi, S., Massari, C., Brocca, L., De Lannoy, G.J.M., 2024. Irrigation Quantification Through Backscatter Data Assimilation With a Buddy Check Approach. *Journal of Advances in Modeling Earth Systems* 16, e2023MS003661. <https://doi.org/10.1029/2023MS003661>
- Dari, J., Brocca, L., Modanesi, S., Massari, C., Tarpanelli, A., Barbetta, S., Quast, R., Vreugdenhil, M., Freeman, V., Barella-Ortiz, A., Quintana-Seguí, P., Bretreger, D., Volden, E., 2023. Regional data sets of high-resolution (1 and 6&thinsp;km) irrigation estimates from space. *Earth System Science Data* 15, 1555–1575. <https://doi.org/10.5194/essd-15-1555-2023>
- Dari, J., Brocca, L., Quintana-Seguí, P., Escorihuela, M.J., Stefan, V., Morbidelli, R., 2020. Exploiting High-Resolution Remote Sensing Soil Moisture to Estimate Irrigation Water Amounts over a Mediterranean Region. *Remote Sensing* 12, 2593. <https://doi.org/10.3390/rs12162593>
- Dari, J., Quintana-Seguí, P., Morbidelli, R., Saltalippi, C., Flammini, A., Giugliarelli, E., Escorihuela, M.J., Stefan, V., Brocca, L., 2022. Irrigation estimates from space: Implementation of different approaches to model the evapotranspiration contribution within a soil-moisture-based inversion algorithm. *Agricultural Water Management* 265, 107537. <https://doi.org/10.1016/j.agwat.2022.107537>
- De Lannoy, G.J.M., Bechtold, M., Busschaert, L., Heyvaert, Z., Modanesi, S., Dunmire, D., Lievens, H., Getirana, A., Massari, C., 2024. Contributions of Irrigation Modeling, Soil Moisture and Snow Data Assimilation to High-Resolution Water Budget Estimates Over the Po Basin: Progress Towards Digital Replicas. *Journal of Advances in Modeling Earth Systems* 16, e2024MS004433. <https://doi.org/10.1029/2024MS004433>
- Dorigo, W., Wagner, W., Albergel, C., Albrecht, F., Balsamo, G., Brocca, L., Chung, D., Ertl, M., Forkel, M., Gruber, A., Haas, E., Hamer, P.D., Hirschi, M., Ikonen, J., de Jeu, R., Kidd, R., Lahoz, W., Liu, Y.Y., Miralles, D., Mistelbauer, T., Nicolai-Shaw, N., Parinussa, R., Pratola, C., Reimer, C., van der Schalie, R., Seneviratne, S.I., Smolander, T., Lecomte, P., 2017. ESA CCI Soil Moisture for improved Earth system understanding: State-of-

the art and future directions. *Remote Sensing of Environment, Earth Observation of Essential Climate Variables* 203, 185–215. <https://doi.org/10.1016/j.rse.2017.07.001>

Entekhabi, D., Njoku, E.G., O'Neill, P.E., Kellogg, K.H., Crow, W.T., Edelstein, W.N., Entin, J.K., Goodman, S.D., Jackson, T.J., Johnson, J., Kimball, J., Piepmeier, J.R., Koster, R.D., Martin, N., McDonald, K.C., Moghaddam, M., Moran, S., Reichle, R., Shi, J.C., Spencer, M.W., Thurman, S.W., Tsang, L., Van Zyl, J., 2010. The Soil Moisture Active Passive (SMAP) Mission. *Proceedings of the IEEE* 98, 704–716. <https://doi.org/10.1109/JPROC.2010.2043918>

Jalilvand, E., Tajrishy, M., Ghazi Zadeh Hashemi, S.A., Brocca, L., 2019. Quantification of irrigation water using remote sensing of soil moisture in a semi-arid region. *Remote Sensing of Environment* 231, 111226. <https://doi.org/10.1016/j.rse.2019.111226>

Jung, M., Koirala, S., Weber, U., Ichii, K., Gans, F., Camps-Valls, G., Papale, D., Schwalm, C., Tramontana, G., Reichstein, M., 2019. The FLUXCOM ensemble of global land-atmosphere energy fluxes. *Sci Data* 6, 74. <https://doi.org/10.1038/s41597-019-0076-8>

Kerr, Y.H., Al-Yaari, A., Rodriguez-Fernandez, N., Parrens, M., Molero, B., Leroux, D., Bircher, S., Mahmoodi, A., Mialon, A., Richaume, P., Delwart, S., Al Bitar, A., Pellarin, T., Bindlish, R., Jackson, T.J., Rüdiger, C., Waldteufel, P., Mecklenburg, S., Wigneron, J.-P., 2016. Overview of SMOS performance in terms of global soil moisture monitoring after six years in operation. *Remote Sensing of Environment, Special Issue: ESA's Soil Moisture and Ocean Salinity Mission - Achievements and Applications* 180, 40–63. <https://doi.org/10.1016/j.rse.2016.02.042>

Martens, B., Miralles, D.G., Lievens, H., van der Schalie, R., de Jeu, R.A.M., Fernández-Prieto, D., Beck, H.E., Dorigo, W.A., Verhoest, N.E.C., 2017. GLEAM v3: satellite-based land evaporation and root-zone soil moisture. *Geoscientific Model Development* 10, 1903–1925. <https://doi.org/10.5194/gmd-10-1903-2017>

Miller, J., Barlage, M., Zeng, X., Wei, H., Mitchell, K., Tarpley, D., 2006. Sensitivity of the NCEP/Noah land surface model to the MODIS green vegetation fraction data set. *Geophysical Research Letters* 33. <https://doi.org/10.1029/2006GL026636>

Modanesi, S., Massari, C., Bechtold, M., Lievens, H., Tarpanelli, A., Brocca, L., Zappa, L., De Lannoy, G.J.M., 2022. Challenges and benefits of quantifying irrigation through the assimilation of Sentinel-1 backscatter observations into Noah-MP. *Hydrology and Earth System Sciences* 26, 4685–4706. <https://doi.org/10.5194/hess-26-4685-2022>

Muñoz-Sabater, J., Dutra, E., Agustí-Panareda, A., Albergel, C., Arduini, G., Balsamo, G., Boussetta, S., Choulga, M., Harrigan, S., Hersbach, H., Martens, B., Miralles, D.G., Piles, M., Rodríguez-Fernández, N.J., Zsoter, E., Buontempo, C., Thépaut, J.-N., 2021. ERA5-Land: a state-of-the-art global reanalysis dataset for land applications. *Earth System Science Data* 13, 4349–4383. <https://doi.org/10.5194/essd-13-4349-2021>

Niu, G.-Y., Yang, Z.-L., Mitchell, K.E., Chen, F., Ek, M.B., Barlage, M., Kumar, A., Manning, K., Niyogi, D., Rosero, E., Tewari, M., Xia, Y., 2011. The community Noah land surface model with multiparameterization options

---

(Noah-MP): 1. Model description and evaluation with local-scale measurements. *Journal of Geophysical Research: Atmospheres* 116. <https://doi.org/10.1029/2010JD015139>

Ozdogan, M., Rodell, M., Beaudoin, H.K., Toll, D.L., 2010. Simulating the Effects of Irrigation over the United States in a Land Surface Model Based on Satellite-Derived Agricultural Data. *Journal of Hydrometeorology* 11, 171–184. <https://doi.org/10.1175/2009JHM1116.1>

Senay, G., 2018. Satellite Psychrometric Formulation of the Operational Simplified Surface Energy Balance (SSEBop) Model for Quantifying and Mapping Evapotranspiration. *Applied Engineering in Agriculture* 34, 555–566. <https://doi.org/10.13031/aea.12614>

Siebert, S., Henrich, V., Frenken, K., Burke, J., 2013. Update of the digital global map of irrigation areas to version 5. <https://doi.org/10.13140/2.1.2660.6728>

Teluguntla, P., Thenkabail, P., Oliphant, A., Gumma, M., Aneece, I., Foley, D. and McCormick, R. (2023). Landsat-derived Global Rainfed and Irrigated-Cropland Product @ 30-m (LGRIP30) of the World (GFSADLGRIP30WORLD). The Land Processes Distributed Active Archive Center (LP DAAC) of NASA and USGS. Pp. 103. IP-148728. DOI: <https://doi.org/10.5067/Community/LGRIP/LGRIP30.001>

Zappa, L., Dari, J., Modanesi, S., Quast, R., Brocca, L., De Lannoy, G., Massari, C., Quintana-Seguí, P., Barella-Ortiz, A., Dorigo, W., 2024. Benefits and pitfalls of irrigation timing and water amounts derived from satellite soil moisture. *Agricultural Water Management* 295, 108773. <https://doi.org/10.1016/j.agwat.2024.108773>

Zappa, L., Schlaffer, S., Bauer-Marschallinger, B., Nendel, C., Zimmerman, B., Dorigo, W., 2021. Detection and Quantification of Irrigation Water Amounts at 500 m Using Sentinel-1 Surface Soil Moisture. *Remote Sensing* 13, 1727. <https://doi.org/10.3390/rs13091727>

Zappa, L., Schlaffer, S., Brocca, L., Vreugdenhil, M., Nendel, C., Dorigo, W., 2022. How accurately can we retrieve irrigation timing and water amounts from (satellite) soil moisture? *International Journal of Applied Earth Observation and Geoinformation* 113, 102979. <https://doi.org/10.1016/j.jag.2022.102979>

Zaussinger, F., Dorigo, W., Gruber, A., Tarpanelli, A., Filippucci, P., Brocca, L., 2019. Estimating irrigation water use over the contiguous United States by combining satellite and reanalysis soil moisture data. *Hydrology and Earth System Sciences* 23, 897–923. <https://doi.org/10.5194/hess-23-897-2019>